EARTH SURFACE PROCESSES AND LANDFORMS
Earth Surf. Process. Landforms **34**, 1339–1352 (2009)

Published online 16 June 2009 in Wiley InterScience
(www.interscience.wiley.com) DOI: 10.1002/esp.1821

Influence of rock mass strength on the erosion rate of alpine cliffs

Jeffrey R. Moore,[1,3] Johnny W. Sanders,[2] William E. Dietrich[2] and Steven D. Glaser[1]
[1] Department of Civil and Environmental Engineering, University of California, Berkeley, California, USA
[2] Department of Earth and Planetary Science, University of California, Berkeley, California, USA
[3] Geological Institute, Swiss Federal Institute of Technology, Zürich, Switzerland

Received 6 October 2008; Revised 25 February 2009; Accepted 9 March 2009

* Correspondence to: Jeffrey R. Moore, Geological Institute, Swiss Federal Institute of Technology, Zürich, Switzerland.
E-mail: jeffrey.moore@erdw.ethz.ch

ESPL
Earth Surface Processes and Landforms

ABSTRACT: Collapse of cliff faces by rockfall is a primary mode of bedrock erosion in alpine environments and exerts a first-order control on the morphologic development of these landscapes. In this work we investigate the influence of rock mass strength on the retreat rate of alpine cliffs. To quantify rockwall competence we employed the Slope Mass Rating (SMR) geomechanical strength index, a metric that combines numerous factors contributing to the strength of a rock mass. The magnitude of cliff retreat was calculated by estimating the volume of talus at the toe of each rockwall and projecting that material back on to the cliff face, while accounting for the loss of production area as talus buries the base of the wall. Selecting sites within basins swept clean by advancing Last Glacial Maximum (LGM) glaciers allowed us to estimate the time period over which talus accumulation occurred (i.e. the production time). Dividing the magnitude of normal cliff retreat by the production time, we calculated recession rates for each site. Our study area included a portion of the Sierra Nevada between Yosemite National Park and Lake Tahoe. Rockwall recession rates determined for 40 alpine cliffs in this region range from 0·02 to 1·22 mm/year, with an average value of 0·28 mm/year. We found good correlation between rockwall recession rate and SMR which is best characterized by an exponential decrease in erosion rate with increasing rock mass strength. Analysis of the individual components of the SMR reveals that joint orientation (with respect to the cliff face) is the most important parameter affecting the rockwall erosion rate. The complete SMR score, however, best synthesizes the lithologic variables that contribute to the strength and erodibility of these rock slopes. Our data reveal no strong independent correlations between rockwall retreat rate and topographic attributes such as elevation, aspect, or slope angle. Copyright © 2009 John Wiley & Sons, Ltd.

KEYWORDS: rockfall; bedrock erosion; alpine cliffs; rock mass strength

Introduction

Rockfall is one of the primary erosional mechanisms controlling the morphologic development of alpine landscapes (Matthes, 1930; Rapp, 1960a, 1960b; Gardner, 1969; Luckman, 1976; Whalley, 1984; Augustinus, 1995a; Ballantyne, 2002). Intense erosion during successive glacial cycles creates oversteepened headwalls and valley flanks that are prone to rapid degradation and collapse. Understanding the mechanisms by which rock slopes erode is a critical step towards process-based modeling of alpine terrain.

In this work, we use the terms cliff, rock slope, rock face, and rockwall interchangeably to describe the same landform: an exposed bedrock slope inclined greater than about 40° and in some cases overhanging. By this definition the dip of the rock face is sufficiently steep to allow gravity-driven transport of loose material and also to prevent significant long-term deposition or storage on the wall (Gerber, 1980).

Rock slope stability is known to be controlled by the mechanical properties and state of stress of the rock mass, as well as the processes that act to degrade the cliff material. Intact rock strength, the presence and geometry of discontinuities (frequency, orientation, persistence, aperture, roughness, infilling), and the rockwall environment (degree of weathering, amount of water or vegetation) combine to control the mechanical behavior of a rock slope (Rapp, 1960a; Terzaghi, 1962a; Selby, 1982; Olyphant, 1983; Bieniawski, 1989; Douglas *et al.*, 1991; Augustinus, 1995b; Weissel and Seidl, 1997; Ballantyne, 2002; Coe and Harp, 2007). These physical characteristics are in a state of constant transition as natural processes attack the rock. The extent of rock mass degradation is a function of the dominant processes acting on the wall (examples include mechanical weathering by ice, chemical weathering by mineral hydration and salt deposition, thermal stresses, and biotic processes), which in turn are a response to the physiography and environmental conditions at each site. Complex interactions between topography and climate have led many researchers to combine them into one variable commonly referred to as topoclimate, which includes elevation, aspect, inclination, temperature, precipitation, and prevailing wind, and which can have a large impact on the rate of rockwall weathering and retreat (Gardner, 1969; Olyphant, 1983; Davies

et al., 2001; Hales and Roering, 2005; Huisman *et al.*, 2006; Gruber and Haeberli, 2007). The state of stress of the rock mass may be affected by removal of overburden or by topographic and tectonic stresses, and can set or alter the rock slope's mechanical properties, often predisposing a particular failure mode (Holzhausen, 1989; Augustinus, 1995a; Miller and Dunne, 1996; Molnar, 2004; Mandl, 2005; Molnar *et al.*, 2007).

Researchers have previously used talus deposits to estimate rockwall erosion rates and constrain landscape evolution models and basin-scale sediment budgets (e.g. Rapp, 1960a, 1960b; Saunders and Young, 1983; Frich and Brandt, 1985; Augustinus, 1995a; Hinchliffe and Ballantyne, 1999; Campbell and Church, 2003; Dadson and Church, 2005; Krautblatter and Dikau, 2007). Several observational investigations led to improved understanding of the factors influencing rockfall initiation and its spatial distribution in alpine landscapes (e.g. Rapp, 1960a, 1960b; Bjerrum and Jorstad, 1968; Luckman, 1976; Gardner, 1983; Whalley, 1984; Wieczorek and Jäger, 1996; Matsuoka and Sakai, 1999), while other studies concentrated on the mechanisms of rock fracture and block removal from a cliff (e.g. Davidson and Nye, 1985; Walder and Hallet, 1985; Anderson, 1998; Matsuoka, 2001; Ishikawa *et al.*, 2004). The dynamics of blocks falling from a rock face has also been investigated (e.g. Evans and Hungr, 1993; Guzzetti *et al.*, 2002), providing a foundation for rockfall hazard assessment and mitigation in high-risk areas (Wieczorek *et al.*, 1999; Guzzetti *et al.*, 2003; Jaboyedoff *et al.*, 2005).

A critical link remains underdeveloped between engineering knowledge of rock slope mechanics and geomorphic investigations of landscape evolution processes, in particular for questions of process rates. Here we document post-glacial talus accumulation at the base of rock cliffs in the Sierra Nevada of California in order to calculate erosion rates and correlate these rates with a common measure of rock mass strength. We observe a well-defined inverse exponential relationship between recession rate and rock mass strength, with joint orientation exerting the greatest influence on erosion rates. These findings point to the need to include the rock mass fracture pattern, not just frictional and cohesion properties, in building models of bedrock landscape erosion.

Methods

Measuring rock mass strength

The term rock mass is used to encompass the influence of both intact material pieces and discontinuities on the overall strength or deformability of a discontinuous rock medium. While it is relatively straightforward to test the mechanical properties of either intact rock or joints individually, describing their interaction is difficult since large volumes of material are required for testing. Several empirical rating schemes are available to quantify the strength of a rock mass.

The Rock Mass Rating (RMR) system accounts for a number of factors influencing rock mass strength, and may be used to quantify the competence of tunnel walls, cliffs, or other rock formations. Created by Bieniawski (1973, 1989), RMR uses the following six parameters: (1) uniaxial compressive strength (UCS), (2) rock quality designation (RQD; Deere, 1963), (3) joint spacing, (4) joint condition, including persistence, aperture, roughness, infilling, and weathering, (5) groundwater conditions, and (6) joint orientation. (Note: the Rock Mass Strength index of Selby (1980) uses essentially the same input parameters as RMR.) RMR scores range from 0 to 100, where a score of 100 represents the most competent rock mass. Scores are derived from a predetermined set of parameter ranges and the RMR is the sum of the six inputs listed earlier. RMR was selected in this study because of its versatility over a wide range of rock types and cliff morphologies, and because it is quickly measured in the field. RMR has also been refined and validated by many case histories from engineering practice (Bieniawski, 1989).

The rating adjustment for joint orientation is paramount for evaluating the competence of a rock slope (Goodman, 1989). The orientation of joints with respect to the rockwall influences slope stability by enabling or preventing block removal by sliding or toppling (Goodman and Shi, 1985). Joints that dip out of the slope, or 'daylight' on the slope, can more easily accommodate sliding and are unfavorable for cliff stability.

Although RMR includes a penalty for unfavorably oriented joints, the point reduction is highly sensitive to user judgment or inexperience, and can sometimes dominate the overall RMR score. Romana (1985, 1995) addressed this shortcoming by introducing the Slope Mass Rating (SMR) system. SMR retains the basic structure of RMR but also provides a quantitative approach for evaluating the joint orientation rating adjustment. SMR addresses both planar sliding and toppling failure modes (Table I); no additional consideration is made for sliding on multiple joint planes. SMR also accounts for the method of slope excavation.

In order to determine the SMR of a rockwall, the RMR is first found using the methodology outlined by Bieniawski (1989), and then the SMR scheme is used to modify the RMR for slope-specific variables. Sections 1–5 of Table I outline the input values and scores for each parameter used to evaluate the RMR, and these five inputs are summed to calculate the unadjusted RMR. In this study, we estimated UCS in the field using an N-type Schmidt hammer (ISRM, 1978), while joint spacing and RQD were measured along a representative scan line (or lines) at the base of the cliff. For multiple scan line cases, parameter values were averaged. Table I, section 6, outlines the input parameters and ranges used to calculate the penalization to the RMR score based on the presence of adversely oriented joints (Romana, 1985, 1995). Finally, Table I, section 7 (parameter F_4) describes the rating adjustment for the method of rock slope excavation, which was constant throughout this work since all our sites are natural rockwalls. The final SMR score is then calculated as:

$$\mathrm{SMR} = \mathrm{RMR} + (F_1 \cdot F_2 \cdot F_3) + F_4 \quad (1)$$

where F_1 through to F_3 are parameters describing the rock slope and joint set geometries, including comparisons evaluating parallelism and the potential for daylighting (see Table I, section 6).

A rock mass generally has at least three prominent joint sets, and to determine the SMR for each cliff the controlling set must be identified. When the critical joint set is not known, the orientation of each must be recorded and the minimum calculated SMR used. For convenience in this study, we define a new variable, JP, which describes the cumulative penalization for adverse joint orientation:

$$\mathrm{JP} = (F_1 \cdot F_2 \cdot F_3) \quad (2)$$

JP includes all SMR calculations concerning the orientation of the controlling joint set, but excludes consideration for the method of slope exposure (F_4), since in this work all cliffs were natural slopes.

Exfoliation (or sheet) joints that parallel topography are common in the granitic rocks of the Sierra Nevada, and have important implications for slope stability (e.g. Matthes, 1930; Terzaghi, 1962b; Holzhausen, 1989). SMR accounts for these

DOI: 10.1002/esp

Table I. The Slope Mass Rating (SMR) system and parameter scoring guidelines (after Bieniawski, 1989; Romana, 1995)

1	Uniaxial compressive strength of intact rock		>250 MPa	100–250 MPa	50–100 MPa	25–50 MPa	<25 MPa
	Rating		15	12	7	4	2
2	Rock quality designation		90–100%	75–90%	50–75%	25–50%	<25%
	Rating		20	17	13	8	3
3	Joint spacing		>2 m	0·6–2 m	200–600 mm	60–200 mm	<60 mm
	Rating		20	15	10	8	5
4	Joint condition	Persistence	<1 m	1–3 m	3–10 m	10–20 m	>20 m
		Rating	6	4	2	1	0
		Aperture	None	<0·1 mm	0·1–1·0 mm	1–5 mm	>5 mm
		Rating	6	5	4	1	0
		Roughness	Very rough	Rough	Slightly	Smooth	Slickensided
		Rating	6	5	3	1	0
		Infilling	None	Hard < 5 mm	Hard > 5 mm	Soft < 5 mm	Soft > 5 mm
		Rating	6	4	2	2	0
		Weathering	Unweathered	Slightly	Moderately	Highly	Decomposed
		Rating	6	5	3	1	0
5	Groundwater	Joint	Dry	Stained	Damp	Wet	Wet
		Flow	No	No	No	Occasional	Continuous
		Description	Completely dry	Damp	Wet	Dripping	Flowing
		Rating	15	10	7	4	0
6	Rating adjustment for joint orientation[a]	Planar: $\lvert\alpha_j - \alpha_s\rvert$ Toppling: $\lvert\alpha_j - \alpha_s - 180\rvert$	>30°	30°–20°	20°–10°	10°–5°	<5°
		F_1	0·15	0·40	0·70	0·85	1·00
		Planar: $\lvert\beta_j\rvert$	<20°	20°–30°	30°–35°	35°–40°	>45°
		F_2[b]	0·15	0·40	0·70	0·85	1·00
		Planar: $\beta_j - \beta_s$	>10°	10°–0°	0°	0°–(–10°)	<–10°
		Toppling: $\beta_j + \beta_s$	<110°	110°–120°	>120°	–	–
		F_3	0	–6	–25	–50	–60
7	Method of slope excavation		Natural	Presplitting	Smooth blasting	Blasting or mechanical	Deficient blasting
		F_4	+15	+10	+8	0	–8

[a] α_j = joint dip direction, α_s = cliff dip direction, β_j = dip of joint, β_s = dip of cliff.
[b] For toppling $F_2 = 1{\cdot}00$.

joints like any other, but their slope-parallel orientation results in a significant score reduction (large JP). Measuring the spacing of exfoliation joints normal to the slope was often difficult and scan lines were rarely feasible. In these cases, we estimated the surficial joint spacing (since spacing increases with depth) from nearby exposures and different cliff facets.

For more detailed information on RMR and SMR the reader is referred to Bieniawski (1989) and Romana (1985, 1995). Application of these rock mass rating schemes to cliffs in our study area is more thoroughly discussed in Moore (2007), with emphasis on field measurement considerations.

Measuring rockwall recession rate

The magnitude of rockwall retreat normal to the cliff face was calculated by: (1) measuring the volume of accumulated talus at the base of the rockwall, (2) compensating for the density difference between talus and intact rock, and (3) dividing by the time-averaged production area of the rock face. In order to convert the magnitude of rockwall retreat to an erosion rate, we selected sites where we were able to constrain the age of the talus deposit (herein called the production time). To that end, we only chose cliffs well within the limit of glacial occupancy during the Last Glacial Maximum (LGM). These recently deglaciated environments provide a unique venue for studying rockwall retreat since debris is generally removed from the bedrock basins during each glaciation, and the advance or retreat history of each glacial cycle is fairly well known (Matthes, 1930; Ballantyne, 2002).

For simplicity, we reduced the site geometry to two dimensions by removing the along-strike width of the cliff and talus pile. A diagrammatic cross-section is illustrated in Figure 1. The geometric variables measured in the field were: dip of talus pile surface (Θ_t), length of talus pile (L_t), angle between toe of talus and top of cliff (Θ_c), and length from toe of talus to top of cliff (L_c). We then calculated the cliff dip angle (Θ_r) and the downslope cliff length (L_r) by:

$$\Theta_r = \tan^{-1}\left[\frac{L_c \sin\Theta_c - L_t \sin\Theta_t}{L_c \cos\Theta_c - L_t \cos\Theta_t}\right] \quad (3)$$

$$L_r = \left[(L_c \sin\Theta_c - L_t \sin\Theta_t)^2 + (L_c \cos\Theta_c - L_t \cos\Theta_t)^2\right]^{\frac{1}{2}} \quad (4)$$

Length parameters were measured with a laser rangefinder and angles with an inclinometer. When possible, we made direct measurements of the cliff face dip and cliff slope length. In a few instances, the cliff length required adjustment for additional debris production from steeply dipping rock slopes above the cliff, so we used a topographic map to estimate the

DOI: 10.1002/esp

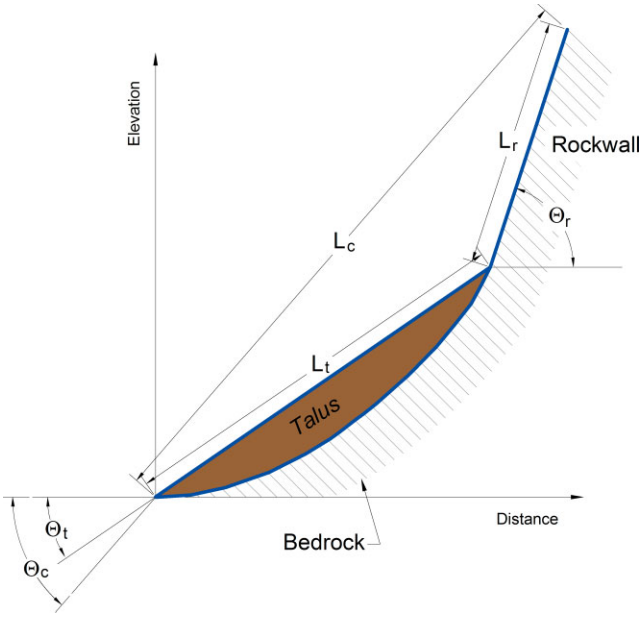

Figure 1. Cross-section of a typical rockwall and talus deposit including the geometric variables measured in the field: dip of talus pile surface (Θ_t), length of talus pile (L_t), angle between toe of talus and top of cliff (Θ_c), and length from toe of talus to top of cliff (L_c). We then calculated the cliff dip angle (Θ_r) and the downslope cliff length (L_r) using Equations 3 and 4. This figure is available in colour online at www.interscience.wiley.com/journal/espl

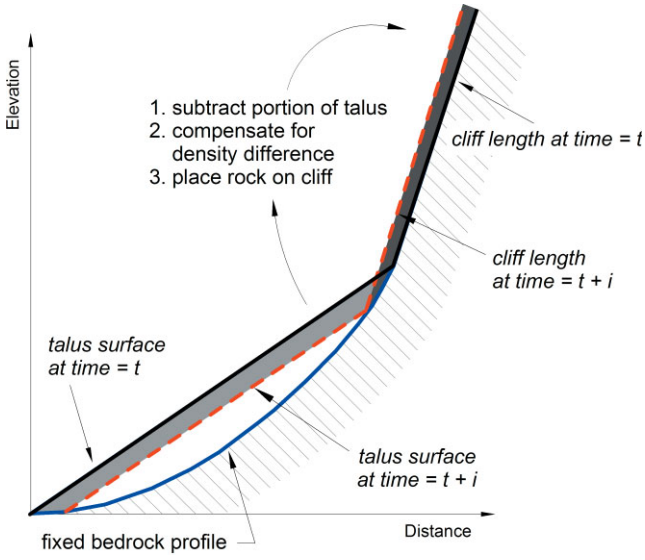

Figure 2. Sketch of the methodology used to calculate the time-averaged downslope cliff length for each rockwall. The initial bedrock and talus profiles are established by the measured and estimated field geometry. In each time increment (i), debris is taken from the talus pile and distributed evenly onto the cliff. The talus surface is lowered in each successive time step and the cliff length elongated. The cliff length is recorded at each interval and the mean value determined at the end of the simulation. This figure is available in colour online at www.interscience.wiley.com/journal/espl

additional production length. Further, some talus slopes had more complex geometries than the simplified form shown in Figure 1 (such as surface concavity or gaps), which we approximated with multiple linear segments.

The bedrock profile beneath each talus deposit was unknown and therefore carefully estimated based on field observations. Nearby outcrops and slope forms, as well as occasional bedrock outcrops within the talus, helped us constrain this profile and estimate talus thickness. The bedrock profiles used in this study may be generalized into three categories: linear, parabolic, and multi-segment. A linear sub-talus profile is the simplest assumption and appropriate when no information about the interface is available (Olyphant, 1983). Parabolic cross-valley morphology (Figure 1) is common in glaciated terrain resulting from the erosive action of glaciers (Graf, 1971; Harbor *et al.*, 1988). In general, we assigned larger rockwalls a parabolic bedrock profile, while smaller cliffs (a few meters high) were approximated by linear forms. Irregular bedrock surfaces, including steps or benches, were used only when there was sufficient field evidence to accurately constrain these forms.

The cross-sectional area of each talus deposit was determined from scaled cross-sections using CAD software. This graphical approach allowed easy analysis of complex talus and bedrock profiles. We calculated the cross-sectional area of intact rock removed from the cliff by multiplying the talus area by the ratio of talus bulk density to intact rock density. The bulk density of a talus deposit depends on the block geometry and size distribution. For the blocky and relatively fresh deposits in this study we assumed a talus bulk density of 1·8 g/cm^3 (Sass and Wollny, 2001; Hales and Roering, 2005), and an intact rock density of 2·65 g/cm^3 (Goodman, 1989). These values imply volumetric bulking by a factor of about 1·5 as intact cliff material is converted to talus.

We treat cliff erosion by rockfall as a time-invariant physical process where material is removed from any exposed bedrock surface. If the rockwall production area is constant through time, the erosion rate is trivial to compute. However, talus accumulation at the base of a cliff progressively buries the wall such that basal portions no longer produce debris (Fisher, 1866). After sufficient time, the rock slope may even become completely mantled and halt talus production altogether (Carson and Kirkby, 1972; Olyphant, 1983). By creating a numerical model of talus reduction, in which debris was incrementally removed from the deposit and reattached to the wall, we were able to simulate snapshots of each cliff through time and calculate the time-averaged production area (or downslope cliff length for cross-sections). This modeling approach allowed us to determine the time-averaged downslope cliff length for each site, which was necessary in order to calculate the long-term average erosion rate. The methodology is outlined in Figure 2 and described below.

The two-dimensional numerical model of talus reduction operated on a predetermined horizontal interval that varied with site dimensions. We first approximated the site-specific bedrock profile beneath and above each talus pile as a polynomial equation using linear regression to fit the field-estimated and measured profile data. The talus surface was described by either a single line or a combination of up to three linear segments. The model iterated in time steps ranging from 10 years (for smaller sites) to 200 years (for the largest site). During each iteration a portion of material (a function of the cliff length and specified erosion rate) was removed from the talus pile, and after applying the density compensation, distributed evenly over the length of the cliff (Figure 2). Through time the rockwall advanced normally outwards and remained parallel to the original cliff profile. In the successive time steps, the surface of the talus was lowered, the cliff length elongated, and the process repeated. The model iterated until at least 98% of the talus was removed, and the downslope cliff length was recorded at each time interval. A successful model run required all talus to be removed within ±1 time step of the assumed accumulation time of 13 000 years (discussed later). If, however, for a selected cliff erosion rate the model removed all talus

DOI: 10.1002/esp

Figure 3. Peak 10 627 in Yosemite National Park is an example of an ideal rockwall study site. The talus deposit is clearly defined (outlined on the image) and sits atop glacier-scoured bedrock. Talus is derived only from the adjoining cliff, and the rockwall geometry and lithology are consistent along strike, allowing the site to be simplified with cross-sections. The inset image shows a closer view of the cliff and talus deposit. This figure is available in colour online at www.interscience.wiley.com/journal/espl

before the specified 13 000 year period, we decreased the erosion rate and repeated the iterative procedure until the time period for talus removal matched. The time-averaged downslope cliff length was then calculated as the mean of the cliff length values for all time increments in the successful simulation.

Unintended model behavior was encountered for linear slope forms. When the model attempted to place new material on the rockwall in these simulations, it first had to create a series of small vertical steps in order to achieve sufficient elevation to support the intact rock thickness while keeping the rockwall profile parallel to the original slope. The resulting cliff profile had a slight concavity at its base, which introduced minor error into the time-averaged cliff length determined for these sites. The model produced the best results for parabolic bedrock profiles.

The average amount of cliff recession normal to the face was calculated by dividing the cross-sectional area of intact material removed from the rockwall by the time-averaged downslope cliff length. Finally, the rockwall recession rate was found by dividing the amount of cliff recession by the production time. Radiocarbon and cosmogenic radionuclide data suggest that glaciers evacuated the basins of the Sierra Nevada between 12 000 to 14 000 years ago, following the resurgent Recess Peak glaciation (Clark and Gillespie, 1997; James *et al.*, 2002). We therefore used a production time of 13 000 years throughout all calculations, despite the fact that the deglaciation date would have varied based on site elevation and aspect (e.g. Guido *et al.*, 2007).

Additional considerations and selection of study sites

Transport of debris from a rock slope (in the absence of glaciers) can be roughly classified into two categories: semi-continuous small rockfall and large stochastic mass wasting (Rapp, 1960a, 1960b; Bjerrum and Jorstad, 1968; Whalley, 1984; Selby, 1993). By calculating the recession rate over a 13 000 year period we hope to capture the long-term rock slope behavior and average out variations caused by episodic slope adjustment. It is possible that cliff erosion rates are relatively rapid immediately following deglaciation and then decrease with time (e.g. Ballantyne, 2002), but we cannot assess this temporal variation from the data obtained in this work.

Careful selection of field sites was critical. It was essential that the most recent glacial advance swept the basin clean of debris, validating our assumption that all observed talus originated since glacial retreat. Weathered and rounded boulders, the presence of copious sand, or weathering forms like gnammas (Matthes, 1930; Twidale, 1965) indicated that the debris preceded the LGM. Ideal sites exhibited: (a) clearly defined talus deposits containing material derived only from the adjacent rockwall, (b) consistent along-strike geometry, (c) simple cliff and talus geometry, (d) unmodified talus piles, and (e) constant lithology throughout the production zone. Figure 3 shows an example of an ideal rockwall study site.

The rockwall recession rate is assumed to be constant along the strike of the cliff. In most cases this simplification is valid, but many alpine cliffs experience erosion by debris flows, deep seated failures, and other localized processes that do not satisfy our spatial erosion assumptions (Whalley, 1984; Luckman, 1992). We specifically avoided cliffs exhibiting deep chutes or gullies where a constant along-strike recession rate appeared invalid.

Talus deposits may be modified by weathering and transport processes, for example slope wash, frost heave, creep, and fluvial incision (Rapp, 1960a; Gerber and Scheidegger, 1974; Hinchliffe, 1999). These processes not only remove debris from the talus pile, but also alter the bulk density of the deposit. Either outcome invalidates some assumptions in this work, resulting in uncertainty in the estimated erosion rates. We reduced possible errors by carefully avoiding talus deposits that appeared significantly modified by internal or external processes.

Study Area

The Sierra Nevada of California extend for more than 700 km at a northwest trend through the eastern portion of the state from the Mojave Desert to the Cascade Range. Mesozoic granitic rocks dominate the lithology throughout most of the range, which intruded into Paleozoic meta-sedimentary and meta-volcanic strata (Bateman and Wahrhaftig, 1966).

DOI: 10.1002/esp

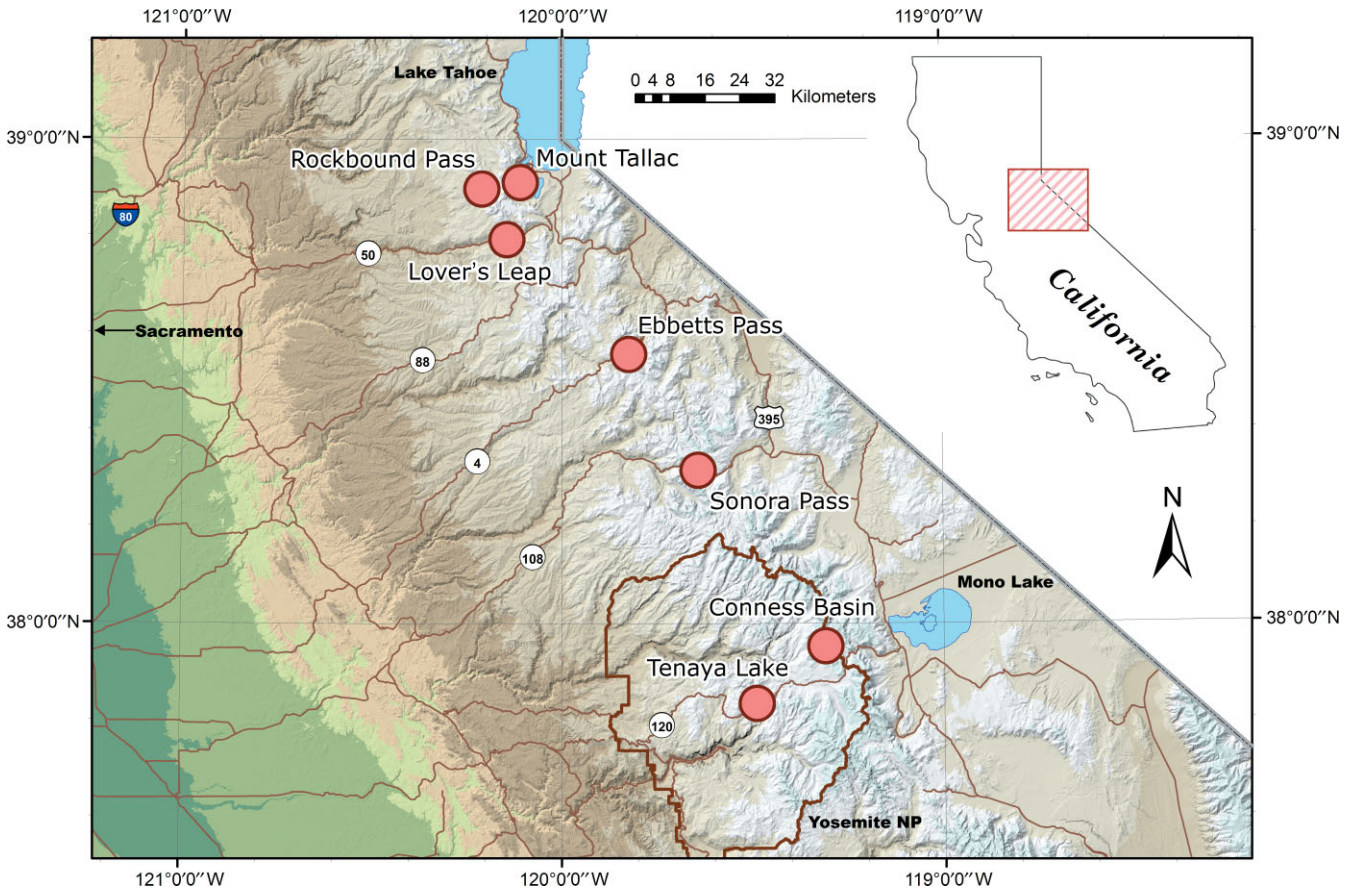

Figure 4. Map showing the location of the study area (inset) and the seven regional focus areas (circles) where multiple rockwall sites were analyzed. This figure is available in colour online at www.interscience.wiley.com/journal/espl

We concentrated on a portion of the northern-central Sierra Nevada between Yosemite National Park and Lake Tahoe (Figure 4). Five major highways transect the range in the study area, and these were used to access the seven regional focus areas shown in Figure 4: Rockbound Pass, Mount Tallac, Lover's Leap, Ebbetts Pass, Sonora Pass, Conness Basin, and Tenaya Lake. We investigated several rockwall sites within each regional focus area. To avoid lithologic bias, we analyzed cliffs composed of granite, granodiorite, diorite, andesite, basalt, and metasedimentary rocks. The rockwalls had mean elevations ranging from 1830 m to 3300 m, downslope cliff lengths (heights) varying from 7 m to 360 m, and were oriented in a variety of aspects.

Radiocarbon and cosmogenic radionuclide dating, combined with moraine superposition, reveal a complex history of repeated glaciations in the Sierra throughout the Quaternary. The most recent glacial episodes are Tioga (~16–31 ka), Recess Peak (~15 ka), and Matthes (Little Ice Age, ~0·65 ka) glaciations (Bateman and Wahrhaftig, 1966; Phillips *et al*., 1996; Clark and Gillespie, 1997; James *et al*., 2002). Except for the small Matthes age advance, the Sierra Nevada may have completely deglaciated with the retreat of the Recess Peak glaciers approximately 13 000 years ago.

Results

Our results show a clear inverse relationship between the measured rockwall recession rate and cliff SMR, where recession rate declines exponentially with increasing rock mass strength (Figure 5). The best fit trend to all data, determined by least squares regression, is given by:

$$\dot{E} = 10{\cdot}25e^{-0{\cdot}065{\cdot}SMR} \quad (5)$$

where the rockwall recession rate ($\dot{E}$) is in mm/year, and the goodness-of-fit parameter (r^2) for the regression is 0·58. Select details of the SMR score and site-specific topographic parameters for each of the 40 rockwall sites are shown in Table II. The cliff, talus, and sub-talus bedrock profiles for each site can be found in Moore (2007).

The rockwall recession rates determined in this work are within the range of previously reported values for alpine regions throughout the world, which generally vary from about 0·1 to 1·0 mm/year (Rapp, 1960a; Carson and Kirkby, 1972; Gray, 1972; Barsch, 1977; Olyphant, 1983; Andre, 1997; Hinchliffe and Ballantyne, 1999; Matsuoka and Sakai, 1999; Sass and Wollny, 2001; Hoffman and Schrott, 2002; Hales and Roering, 2005; Berthling and Etzelmüller, 2007; Sass, 2007). The mean recession rate of the 40 cliffs investigated in this work is 0·28 mm/year, implying that on average, alpine rockwalls in the study area have retreated 3·6 m over the last 13 000 years. The maximum recession rate measured (1·22 mm/year) requires normal cliff retreat of nearly 16 m, while the minimum recession rate (0·02 mm/year) requires only 0·26 m of cliff retreat.

To help elucidate which components of the SMR control our observed relationship with retreat rate (Equation 5), we plotted rockwall recession rate against UCS, joint spacing, joint condition, and the penalization for adverse joint orientation, JP (Figures 6a–6d). Analysis of these four graphs reveals that only JP correlates with the measured erosion rates. Neither joint spacing, joint condition, nor UCS show any discernable trend with rockwall recession rate. We next calculated Pearson product-moment correlation coefficients (PMCC; Borradaile,

DOI: 10.1002/esp

Table II. Details of the SMR score and site-specific topographic and geometric variables for each of the 40 rockwalls studied

Site #	Area	Latitude/Longitude (NAD83)	Lithology	UCS (MPa)	RQD (%)	Joint spacing (m)	Joint condition rating	JP	SMR	Mean elevation (m)	Bearing (azimuth)	Talus area (m^2)	Current cliff slope length (m)	Time-avg. cliff slope length (m)	Cliff dip angle	Talus prod. rate (mm/year)	Rockwall recession rate (mm/year)
1	Conness Basin	37·9763° N, 119·3082° W	granodiorite	108	100	2·13	17	0	92	3262	70	23	52	55	54	0·03	0·02
2		37·9750° N, 119·3033° W	granodiorite	59	97	0·37	15	–8	68	3293	285	160	84	91	53	0·14	0·09
3		37·9797° N, 119·3006° W	granodiorite	123	85	0·22	16	–2	72	3171	105	63	64	71	47	0·07	0·05
4		37·9788° N, 119·3005° W	granodiorite	108	89	0·25	20	–10	69	3201	80	215	98	104	65	0·16	0·11
5		37·9928° N, 119·2870° W	metased·	72	46	0·10	20	–12	56	3140	250	95	13	20	60	0·36	0·25
6		37·9915° N, 119·2871° W	metased·	88	44	0·09	15	–10	55	3171	240	108	17	24	55	0·35	0·24
7		37·9694° N, 119·2758° W	granodiorite	123	20	0·07	17	–9	55	3110	90	404	31	42	56	0·73	0·50
8	L·Leap	38·8006° N, 120·1352° W	granodiorite	59	82	0·20	15	–15	55	1890	324	458	173	182	66	0·19	0·13
9		38·8019° N, 120·1329° W	granodiorite	77	95	0·33	14	–17	58	1890	296	915	85	100	76	0·70	0·48
10	Rockbound Pass	38·8946° N, 120·2065° W	diorite	78	100	0·48	18	–10	71	2378	210	111	25	32	54	0·27	0·18
11		38·8946° N, 120·2060° W	diorite	78	81	0·19	15	–6	66	2378	190	131	21	28	61	0·35	0·24
12		38·8949° N, 120·2022° W	diorite	88	49	0·10	18	–3	66	2390	230	12	7	10	81	0·10	0·06
13		38·8954° N, 120·2003° W	granodiorite	99	100	0·63	17	–4	77	2457	300	171	315	335	65	0·04	0·03
14		38·8925° N, 120·2044° W	diorite	92	71	0·15	17	–3	69	2390	345	22	14	18	45	0·09	0·06
15		38·8928° N, 120·2055° W	diorite	127	100	0·91	18	–6	82	2360	165	3·5	11	12	81	0·02	0·02
16		38·8911° N, 120·2069° W	diorite	106	95	0·33	13	–25	51	2366	300	93	14	16	77	0·45	0·30
17		38·8853° N, 120·1981° W	granodiorite	106	98	0·38	22	–24	63	2530	255	189	26	33	71	0·43	0·30
18		38·8792° N, 120·1928° W	granodiorite	89	92	0·29	18	–13	67	2622	285	97	84	90	37	0·08	0·06
19	Sonora Pass	38·3389° N, 119·8217° W	basalt	99	99	0·40	15	–24	53	1829	252	285	66	74	62	0·30	0·20
20		38·3372° N, 119·8039° W	basalt	100	100	0·43	14	–14	65	1902	290	270	42	51	79	0·41	0·28
		SMR only, band above 20	basalt	76	77	0·17	26	–6	76	1902	290	270	42	51	79	0·41	0·28
21		38·3384° N, 119·8029° W	basalt	84	95	0·33	16	–9	66	1860	20	970	32	59	48	1·26	0·85
22		38·3257° N, 119·7517° W	granite	81	100	0·40	15	–25	54	1951	240	86	17	23	74	0·29	0·20
23		38·3139° N, 119·6675° W	andesite	35	100	0·40	19	–21	59	2805	0	3823	360	394	46	0·75	0·51
24	Ebbetts Pass	38·5655° N, 119·8084° W	andesite	51	27	0·08	21	–19	45	2530	105	378	55	64	75	0·45	0·31
25		38·5665° N, 119·8114° W	andesite	54	86	0·23	16	–11	61	2549	30	348	130	148	40	0·18	0·12
26		38·5473° N, 119·8136° W	basalt	90	19	0·07	15	–23	37	2732	130	885	47	68	54	1·00	0·68
27		38·5481° N, 119·8135° W	basalt	116	67	0·14	22	–21	56	2744	64	61	14	14	89	0·34	0·23
28		38·5483° N, 119·8144° W	basalt	87	0	0·03	24	–14	52	2744	0	370	64	74	60	0·39	0·26
29	Tenaya Lake	37·8190° N, 119·4848° W	granodiorite	72	100	0·50	13	–1	74	2652	300	299	75	84	61	0·27	0·19
30		37·8710° N, 119·4210° W	granodiorite	45	100	0·50	17	–30	49	2683	25	2011	107	134	55	1·15	0·78
31		37·8714° N, 119·4198° W	granodiorite	22	82	0·20	15	–13	53	2683	0	1087	141	169	40	0·50	0·34
32		37·8727° N, 119·4043° W	granodiorite	55	100	0·80	19	–2	81	2774	0	351	315	412	62	0·07	0·04
33		37·8471° N, 119·4428° W	granodiorite	72	85	0·22	13	–30	42	2622	333	1731	34	74	53	1·80	1·22
34		37·8557° N, 119·4988° W	granodiorite	45	95	0·33	12	–10	56	3140	180	198	45	51	53	0·30	0·20
35		37·8556° N, 119·4974° W	granodiorite	67	100	0·45	16	–17	60	3110	180	229	65	71	58	0·25	0·17
36	Mount Tallac	38·8905° N, 120·0858° W	metased	180	50	0·40	16	–15	56	2500	60	114	121	149	47	0·64	0·43
37		38·9405° N, 120·1167° W	granodiorite	52	18	0·07	12	–5	46	2378	300	489	300	344	52	1·18	0·80
38		38·9430° N, 120·1235° W	granodiorite	145	93	0·50	18	–5	77	2134	120	4	21	25	65	0·14	0·09
39		38·9420° N, 120·1247° W	granodiorite	76	78	0·20	15	–5	67	2195	100	29	107	118	65	0·20	0·14
40		38·9502° N, 120·1173° W	granodiorite	100	82	0·30	17	0	82	2073	130	3	11	15	74	0·19	0·13

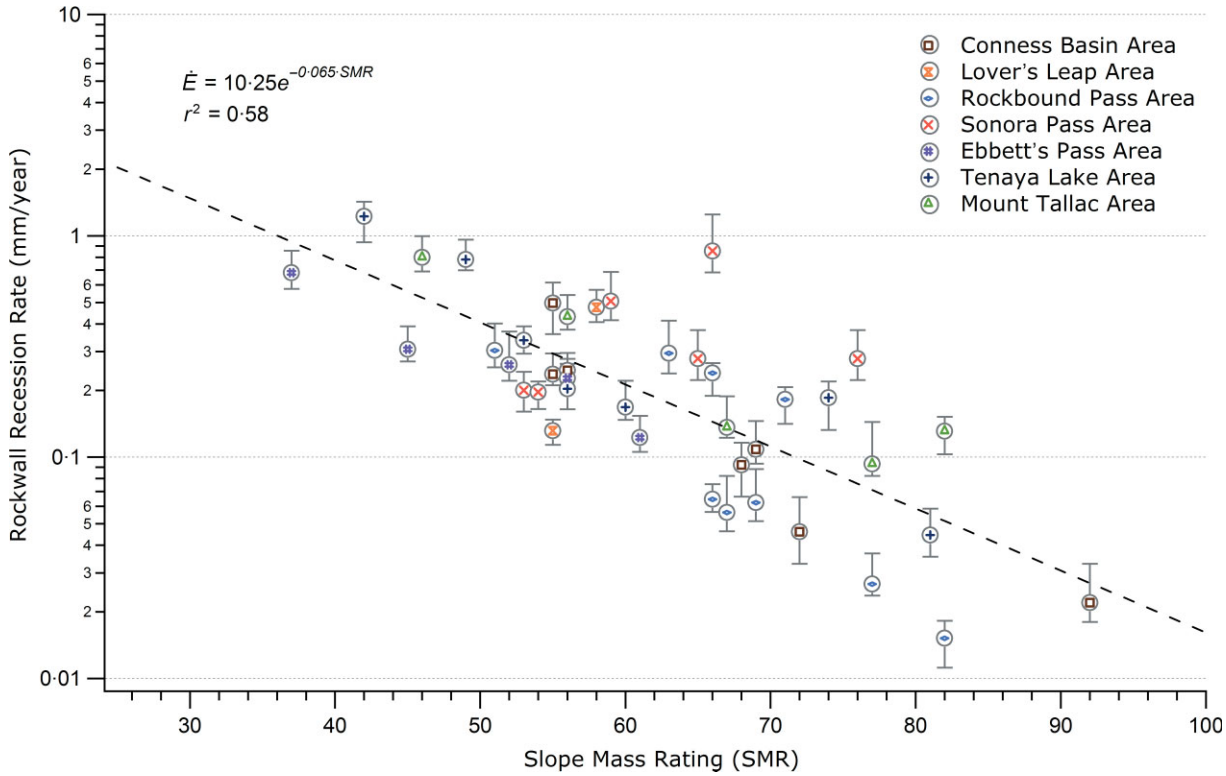

Figure 5. Variation of rockwall recession rate with cliff SMR. Symbols reflect regional focus area. Dashed line shows the exponential best fit trend to all data, and the numerical expression is given. Error bars reflect uncertainty in describing the bedrock profile beneath each talus deposit. Based on repeated measurements at the same cliff, we estimate that each SMR score is accurate to within ±5 points (these error bars not shown for clarity). This figure is available in colour online at www.interscience.wiley.com/journal/espl

Table III. Pearson product-moment correlation coefficient (PMCC) matrix describing the relationships between select rock mass strength and topographic parameters, and the measured rockwall recession rates

	UCS	Joint spacing	Joint condition	JP	SMR	Mean elevation	Aspect	Present slope length	Cliff slope angle	Rockwall recession rate
UCS	1									
Joint spacing	0·17	1								
Joint condition	0·14	–0·04	1							
JP	0·14	0·24	0·03	1						
SMR	0·28	0·61	0·23	0·75	1					
Mean elevation	–0·09	0·12	0·05	0·09	–0·04	1				
Aspect	0·01	–0·14	–0·30	–0·03	–0·04	–0·29	1			
Present slope length	–0·45	0·05	–0·08	0·02	–0·09	0·08	–0·29	1		
Cliff slope angle	0·24	0·005	0·29	–0·08	0·13	–0·40	0·23	–0·35	1	
Rockwall recession rate	–0·20	–0·27	–0·24	–0·54	–0·64	–0·08	–0·04	0·15	–0·20	1

Note: The PMCC ranges from –1 to 1 and is computed as the covariance of the two parameters divided by the product of their standard deviations. Positive values reflect a direct correlation while negative values signify an inverse trend (Borradaile, 2003).

2003) describing the correlation between each rock mass variable and recession rate (Table III). The results confirm that only JP shows considerable correlation with recession rate. This suggests that joint orientation (with respect to the cliff) is the dominant variable controlling rockfall susceptibility and the relationship between SMR and erosion rate for the cliffs studied. The PMCC determined when comparing the complete SMR to erosion rate, however, is greater than with JP alone (–0·64 versus –0·54, respectively), suggesting important contributions from other rock mass properties.

To help assess the role of extrinsic forcings from topoclimate variables on rockwall erosion at each site, we plotted recession rate against mean cliff elevation, rockwall aspect, current slope length, and cliff inclination (Figures 7a–7d). The observed correlations are surprisingly weak, and demonstrate that none of these topoclimate variables independently influence the rockwall retreat rate. Calculated values of the PMCC for each topoclimate parameter confirm that no strong correlations exist with rockwall recession rate in our data set (Table III). For the cliffs studied, rock mass strength therefore appears to be the dominant variable controlling erosion rate, while environmental factors are likely of secondary importance.

Uncertainty in the results of this study comes from both the SMR scoring process and the erosion rate calculation. Factors complicating SMR measurement are discussed in an earlier section and in greater detail by Bieniawski (1989), Romana

DOI: 10.1002/esp

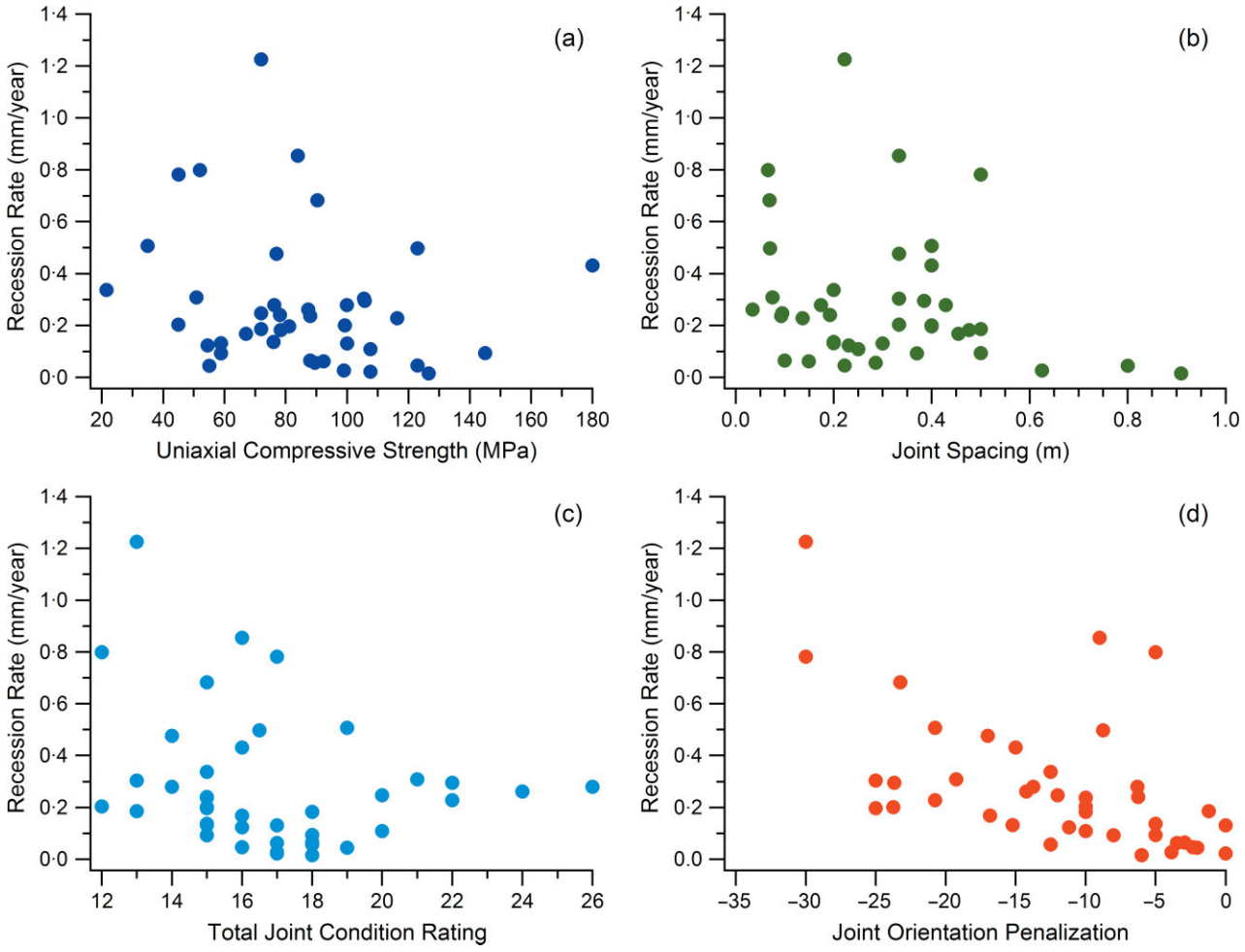

Figure 6. Rockwall recession rate plotted against (a) uniaxial compressive strength, (b) joint spacing, (c) total joint condition rating, and (d) penalization for adverse joint orientation, JP. This figure is available in colour online at www.interscience.wiley.com/journal/espl

(1995), and Moore (2007). Rock mass heterogeneity is inevitable at many spatial scales on a cliff. Nevertheless, the SMR score assigned to each site appears to be accurate to within ±5 points based on repeat measurements taken at different locations along individual cliffs. Given the steep topography at our sites, more extensive sampling was generally not possible.

Error in the rockwall recession rate calculation arises primarily from the difficult task of describing the bedrock profile beneath each talus deposit. Since we have no direct measurement of talus thickness, it is impossible to quantify precisely the error of our best-guess bedrock profile approximation. To investigate the magnitude of the error caused by this uncertainty, we varied our estimation of the bedrock profile at each site within plausible limits (based on our knowledge of the site), and then calculated the resulting change in talus area. Overall, uncertainties ranged from 10% to 55% of the best-guess value, with a mean estimated error of around 25%. Talus area error leads to an equal amount of uncertainty in the rockwall recession rate (see error bars in Figure 5). In most cases we found it more realistic to increase our estimate of talus thickness rather than decrease it, thereby causing the cross-sectional area (and resulting recession rate) to increase.

Another source of error in the recession rate calculation arises from the assumption that the talus production time is fixed at 13 000 years for all sites. Changing this value uniformly does not alter the correlation of erosion rate with SMR. However, spatial variations in the deglaciation age introduce uncertainty in the calculated recession rates. Estimation of the error caused by using a constant talus production time at all sites (determined by varying the production time within a reasonable range) suggests that this assumption may lead to uncertainty of up to 30% in the final value of the rockwall recession rate.

Finally, we note that by selecting sites with well-developed talus deposits and standing cliffs, we introduce an inevitable bias into the results of this study. We frequently encountered small bedrock walls with no talus at their base as well as low-angle rock slopes mantled with talus, but we could not fully include either of these landforms in our inventory.

Discussion

This research addresses how rock mass competence (quantified using the SMR index) affects the rate of cliff erosion by rockfall. One key result is that the rockwall recession rate was found to vary inversely with rock mass strength in an exponential trend. This trend successfully accounts for the expected rock slope behavior at high SMR values, where the erosion rate approaches zero. However, we do not recommend that this trend be used to extrapolate erosion rates at very low SMR. Moon *et al*. (2001) demonstrated that application of rock mass rating systems to weak rock masses (SMR < 20) is only appropriate when the slope fails along joint planes, otherwise the contribution of the intact rock strength is overestimated. Rock mass classification schemes may therefore be unable to quantify accurately the competence of poor-quality rock masses. We have accordingly truncated our plot of rockwall

DOI: 10.1002/esp

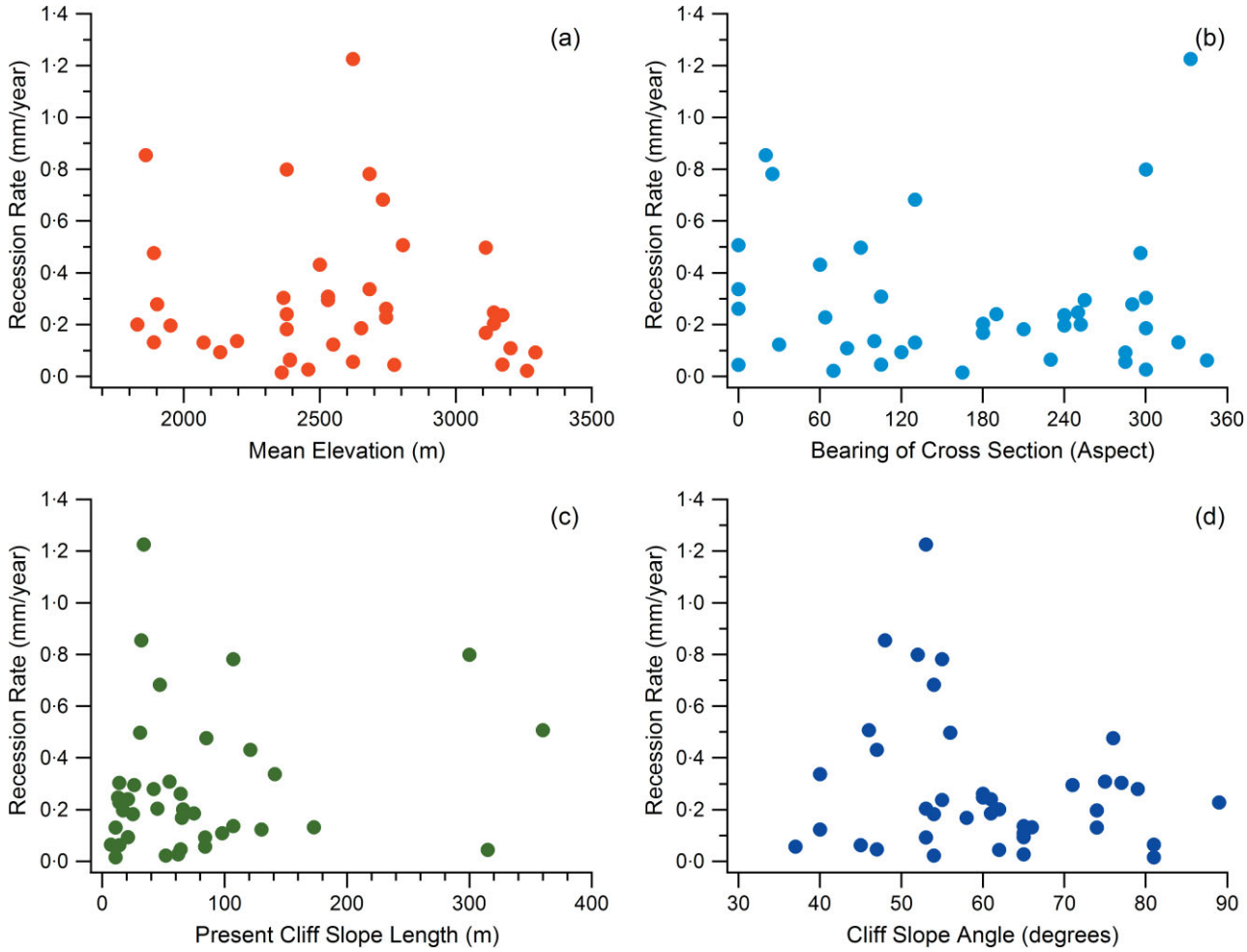

Figure 7. Rockwall recession rate plotted against (a) mean cliff elevation, (b) cliff aspect, (c) present cliff slope length, (d) and cliff slope angle. This figure is available in colour online at www.interscience.wiley.com/journal/espl

recession rate versus SMR (Figure 5) to preclude extrapolation beyond the limits of our data.

The SMR obtained at each site is used to describe the behavior of the entire rock slope above the talus accumulation. For small cliffs, assigning a single SMR to the rock face is reasonable since little spatial heterogeneity exists. However, for large rock slopes this simplification may introduce error. Large cliffs are commonly not monolithologic and may have spatially variable joint and cliff orientations, in addition to local variations in joint spacing and groundwater flow. For heterogeneous bedrock, a single SMR measurement may only capture a portion of the rockwall's mechanical behavior. In a previous study, Selby (1980) showed that variations in rock mass strength along a vertical cliff profile correlated with changing lithology. Similarly in our study, one site in the Sonora Pass area had a layer of horizontal columnar basalt overlying vertically-oriented columnar basalt. SMR measurements of each basalt layer differed by nine points, with the vertically-oriented columns being the weaker of the two (Site 20, Table II). For the remainder of the sites investigated in this work, we minimized error caused by lithologic variation by selecting only cliffs with relatively homogeneous composition.

The correlation between recession rate and SMR suggests that the SMR scheme adequately quantifies the rock mass strength variables that influence the erosion rate of cliffs within our study area. Analysis of the parameters comprising the SMR reveals that the dominant variable controlling the rate of cliff retreat is joint orientation with respect to the rockwall (Figure 6d). Joint orientation controls cliff erodibility by enabling or preventing block removal by sliding or toppling, the dominant failure mechanisms for a discontinuous hard rock slope under gravitational loading (Goodman, 1989). Joints create strong directional rock mass strength anisotropy, so their orientation with respect to the cliff free face critically controls the slope's natural collapse rate (e.g. Coe and Harp, 2007). Blocks liberated by the intersection of multiple joint sets create wedges that can slide if the orientation of the line of intersection daylights on the free face. In our study area, we frequently observed talus cones with apexes at the intersection of two prominent discontinuities. In these cases, the wedge eroded rapidly and progressively deepened, focusing further erosion and creating a gulley.

One rock mass variable commonly correlated to the rate of cliff retreat is joint spacing (e.g. Olyphant, 1983; Andre, 1997). The results of this study (Figure 6b) show that joint spacing alone does not control the rockwall recession rate, and therefore should not be used as a proxy for the erodibility of cliffs. Similarly, intact rock strength, joint condition, and lithology do not appear to be useful independent predictors of rockwall erosion rates in our study area.

Given the versatility of the SMR scheme, it is feasible to use the relationship presented in Equation 5 to estimate the recession rate of other cliffs within the study area. For climatic regions other than the Sierra Nevada, however, this relationship may not be appropriate. Regional climate may be the most important parameter controlling regional rockwall retreat rates (Luckman, 1976; Olyphant, 1983; Hales and Roering, 2005), while rock mass strength perturbations may only

DOI: 10.1002/esp

Table IV. PMCC values describing correlations between select topographic attributes and rockwall recession rate for cliffs of similar strength

	SMR < 50	50 ≤ SMR < 60	60 ≤ SMR < 70	70 ≤ SMR
Mean elevation	0·13	0·17	–0·54	–0·58
Aspect (bearing)	0·64	–0·43	–0·45	0·56
Cliff slope length	0·01	0·42	–0·29	–0·22
Cliff slope angle	–0·79	–0·32	–0·03	0·23

superimpose secondary variability on local erosion rates. The temperature of the rockwall, moisture availability, water pressure in joints, and the principal weathering processes are all influenced by the regional climate. For different climates, a similar inverse trend between rockwall recession rate and SMR may exist, but the magnitude of the erosion rates will likely vary with factors such as the mean annual quantity of rainfall.

One principal conclusion of this research is that the cliff recession rate in our study area depends primarily on rock mass strength. Therefore, to further investigate correlations between topographic attributes (cliff elevation, aspect, length, and inclination) and the rockwall erosion rate, the data were sorted into groups of similar rock mass strength. Four strength groups were created such that there were about 10 data points in each: SMR < 50, 50 ≤ SMR < 60, 60 ≤ SMR < 70, and 70 ≤ SMR (the lowest group contained only five data points). Table IV reports PMCC values describing the correlations between each topographic attribute and rockwall recession rate for the four SMR strength groups. We find no consistent trends across the strength groups, and note irregular PMCC sign reversals signifying changes between direct and inverse correlations.

Rockwall aspect influences the mean annual temperature and the amplitude of diurnal and seasonal temperature fluctuations by controlling topographic shading. Certain aspects also favor the formation and persistence of glaciers, which can act to undercut adjacent rockwalls. Observations by Gardner (1983) in the Canadian Rockies, and by Sass and Wollny (2001) and Sass (2007) in the European Alps suggest that north-facing cliffs erode faster than those of other aspects. In this work, however, we found no consistent correlation between the rockwall aspect and recession rate for cliffs of similar strength (Table IV).

As a result of the regional lapse rate and orographic effect, the temperature and moisture regimes are also a function of elevation. Hales and Roering (2007) suggested that scree production is maximized at a narrow elevation range where the mean annual temperature supports efficient segregation ice growth. Our data do not support this hypothesis, as they reveal no independent trend between cliff elevation and erosion rate (Figure 7a, Table III). Similarly, when sorted into groups of similar rock mass strength, our data do not reveal any consistent trend with elevation (Table IV), or any elevation range where rockwall erosion rates are maximized. We acknowledge, however, that our data do not extend to the highest elevations of the range.

Earthquakes are known to trigger rockfalls over large areas within seismically active mountain belts. For example, the 1980 Mammoth Lakes earthquake sequence triggered thousands of rockfalls and slides in the Sierra Nevada (Harp *et al*., 1984). Similar concentrated rockfall activity also occurs during periods of prolonged intense rainfall (Wieczorek and Jäger, 1996). We can only raise the question of whether these regional triggering factors provide a large enough input to disguise local topoclimate-induced variations in rockfall activity. This may in part explain why we observe no strong trends between cliff retreat rates and topoclimate variables. However, we could equally suggest that variations in rock mass properties related to aspect or elevation might act in concert with these regional triggering mechanisms to enhance rockfall activity in certain locations.

Hillslope transport of soil has been shown to vary with local slope gradient (e.g. McKean *et al*., 1993; Roering *et al*., 1999). Although erosion of bedrock landscapes is fundamentally different, such slope dependencies have been applied to mountains (e.g. Koons, 1989; Tomkin and Braun, 2002, and references therein). Our results, however, do not support application of these expressions to rock cliffs: the interaction of joint orientation and slope, rather than slope alone, is the principal control on rockwall retreat at our sites. For rockwalls of similar strength, we observe no reliable trend between erosion rate and cliff inclination (Table IV). Selby (1980, 1982, 1993) found that for certain configurations, rockwall slope will adjust to rock mass strength, with steeper slopes on stronger rocks. The lack of such correlation in our data (PMCC = 0·13, see Table III) may be due to over-steepening from recent glacial undercutting.

The rate of rock slope modification following glacial retreat and debuttressing has been suggested to be greatest immediately following deglaciation and then decrease with time (Rapp, 1960a; Bjerrum and Jorstad, 1968; Augustinus, 1995b; Wieczorek and Jäger, 1996; Ballantyne, 2002, and references therein; Dadson and Church, 2005). We cannot assess this temporal change with our data. While our average rates for the past 13 000 years are useful measures, the current and future rates may differ as the cliff form changes and as climate shifts.

Implications for Alpine Landscape Evolution

Rockwall processes are among the principle agents of landscape modification in alpine terrain during interglacial cycles and on steep bedrock surfaces above the glacial limit. Rockwall erosion and cliff collapse reshape valleys and distribute colluvium to lower slopes and elevations. Our results are relevant to the development of alpine rockwalls in two complementary ways: (1) the surprising result that local topographic and climatic variations played no discernable role in rockwall erosion in our study area, and (2) to the first order, we found that rock mass strength (and especially discontinuity geometry) controls rockwall recession rate.

The lack of correlation between cliff retreat rate and aspect or elevation raises the question of whether rock fracture by segregation ice growth (e.g. Walder and Hallet, 1985; Anderson, 1998; Matsuoka, 2001; Hales and Roering, 2007) is an important geomorphic agent within our study area. Other mechanisms of joint formation may in fact supersede ice, such as topographic or tectonic stresses, and stress redistribution following deglaciation (Augustinus, 1995a, 1995b; Miller and Dunne, 1996; Mandl, 2005; Molnar *et al*., 2007). Rock mass strength is a metric describing a rockwall's propensity for (rather than the causes of) rockfall. Actual destabilization processes that overcome frictional or cohesive forces resisting freefall depend on a range of environmental variables (e.g. Rapp, 1960a;

DOI: 10.1002/esp

Gardner, 1983; Douglas *et al*., 1991; Matsuoka and Sakai, 1999; Davies *et al*., 2001; Matsuoka, 2001; Ishikawa *et al*., 2004; Gruber and Haeberli, 2007; Krautblatter and Dikau, 2007). A number of potential destabilizers, such as cleft-water pressure, ice-filled discontinuities, earthquakes, wind, and snow and debris avalanches from above, may act independently or in concert on disparate sections of a mountain massif to induce rockfall (Matthes, 1938; Terzaghi, 1962a).

The dependence of rockfall erosion on rock mass mechanical properties highlights two significant improvements necessary for landscape evolution modeling in alpine environments: (1) accurate predictors of joint formation that calculate attributes such as length, aperture, orientation, spacing, and roughness rather than simply crack growth, and (2) erosion laws that incorporate multiple bedrock strength parameters as separate variables (e.g. Tomkin and Braun, 2002). Fracture density, for example, is not sufficient for rockwall erosion rate prediction, as stable configurations exist even in highly fractured slopes (Terzaghi, 1962a). With well-developed alpine geomorphic transport laws (*sensu* Dietrich *et al*., 2003), exploring interactions between slope, aspect, and joint orientation would be possible with the potential for unexpected results; such as, for example, cirque headwall morphology controlled by properties unrelated to glacier mechanics or occupancy, or combinations of slope, aspect, and joint orientation that are impermissible in a landscape because of rapid backwearing. Additionally, efforts to predict sites of joint formation via ice lensing, topographic and tectonic stresses, overburden removal, and freeze–thaw cycles should be expanded to explore how the stresses (and consequent crack growth) interact with or reflect the surface morphology (Savage and Swolfs, 1986; Holzhausen, 1989; Augustinus, 1995a; Miller and Dunne, 1996; Matsuoka, 2001; Molnar, 2004; Hales and Roering, 2007). At this time, Equation 5 could (within the limits mentioned earlier) be used to predict the expected erosion rate of a cliff where the SMR is known, but until rock mass strength can be predicted *a priori*, landscape evolution models will have to make significant assumptions to capture the effects of rockfall in alpine environments (e.g. Irigaray *et al*., 2003; Marquinez *et al*., 2003).

Conclusions

Recession rates calculated from post-glacial talus accumulation for 40 alpine cliffs in the Sierra Nevada ranged from 0·02 to 1·22 mm/year, with an average rate of 0·28 mm/year. These values correspond to between 0·26 and 16 m of normal cliff retreat during the current interglacial period. Rockwall recession rate was found to decrease exponentially with increasing rock mass strength of the cliff production area (as measured by the SMR index). Analysis of the individual parameters comprising the SMR revealed that the penalization for adverse joint orientation is the most important parameter forcing the relationship with rockwall recession rate. Other rock mass properties such as UCS, joint condition, and joint spacing did not correlate well with the rockwall recession rate, indicating that these may be poor predictors of cliff erodibility. The full SMR score best synthesizes the rock mass variables that contribute to the strength and natural collapse rate of the rock slopes studied.

Cliff erosion rates showed no significant correlation with topographic attributes such as elevation, aspect, and cliff slope angle and length, confirming that variations in rockwall recession rates within our study area are primarily controlled by rock mass strength. This presents the important challenge of developing theory for predicting rock mass strength in order to model landscape evolution processes.

Acknowledgements—The authors would like to thank Leslie Hsu and Jan Goethals for help in the field. Kurt Cuffey, T.C. Hales, Greg Stock, and Jeff Coe provided valuable reviews that improved this manuscript. Financial support was provided in part by the Geological Society of America research grant #8078-05, and by the Jane Lewis Foundation.

References

Anderson RS. 1998. Near-surface thermal profiles in alpine bedrock: implications for the frost weathering of rock. *Arctic Alpine Research* **30**: 362–372.

Andre MF. 1997. Holocene rockwall retreat in Svalbard: A triple-rate evolution. *Earth Surface Processes and Landforms* **22**: 423–440.

Augustinus PC. 1995a. Glacial valley cross-profile development: the influence of in situ rock stress and rock mass strength, with examples from the Southern Alps, New Zealand. *Geomorphology* **14**: 87–97.

Augustinus PC. 1995b. Rock mass strength and the stability of some glacial valley slopes. *Zeitschrift für Geomorphologie* **39**: 55–68.

Ballantyne CK. 2002. Paraglacial geomorphology. *Quaternary Science Review* **21**: 1935–2017.

Barsch D. 1977. An estimation of talus production around and transport by active rock glaciers in the Swiss Alps. *Zeitschrift für Geomorphologie, Suppl.-Bd*. **28**: 148–160.

Bateman PC, Wahrhaftig C. 1966. Geology of the Sierra Nevada. *California Division of Mines and Geology Bulletin* **190**: 107–172.

Berthling I, Etzelmüller B. 2007. Holocene rockwall retreat and the estimation of rock glacier age, Prins Karls Forland, Svalbard. *Geografiska Annaler Series A* **89**: 83–93.

Bieniawski ZT. 1973. Engineering classification of jointed rock masses. *Transactions of the South African Institution of Civil Engineers* **15**: 335–344.

Bieniawski ZT. 1989. *Engineering Rock Mass Classifications*. John Wiley and Sons: New York.

Bjerrum L, Jorstad F. 1968. *Stability of Rock Slopes in Norway*, publication 79. Norwegian Geotechnical Institute: Oslo; 1–11.

Borradaile GJ. 2003. *Statistics of Earth Science Data*. Springer-Verlag: New York.

Campbell D, Church M. 2003. Reconnaissance sediment budgets for Lynn Valley, British Columbia: Holocene and contemporary time scales. *Canadian Journal of Earth Sciences* **40**: 701–713.

Carson MA, Kirkby MJ. 1972. *Hillslope Form and Process*. Cambridge University Press: Cambridge.

Clark DH, Gillespie AR. 1997. Timing and significance of late-glacial and Holocene cirque glaciation in the Sierra Nevada, California. *Quaternary International* **38/39**: 21–38.

Coe JA, Harp EL. 2007. Influence of tectonic folding on rockfall susceptibility, American Fork Canyon, Utah, USA. *Natural Hazards and Earth System* Sciences **7**: 1–14.

Dadson SJ, Church M. 2005. Postglacial topographic evolution of glaciated valleys: a stochastic landscape evolution model. *Earth Surfaces Processes and Landforms* **30**: 1387–1403.

Davidson GP, Nye JF. 1985. A photoelastic study of ice pressure in rock cracks. *Cold Regions Science and Technology* **11**: 141–153.

Davies MCR, Hamza O, Harris C. 2001. The effect of rise in mean annual temperature on the stability of rock slopes containing ice-filled discontinuities. *Permafrost and Periglacial Processes* **12**: 137–144.

Deere DU. 1963. Technical description of rock cores for engineering purposes. *Rock Mechanics & Engineering Geology* **1**: 1–18.

Dietrich WE, Bellugi DG, Sklar LS, Stock JD, Heimsath AM, Roering J. 2003. Geomorphic transport laws for predicting landscape form and dynamics. In *Prediction in Geomorphology*, Wilcock P, Iverson R (eds). AGU: Washington, DC; 103–132.

Douglas GR, Whalley WB, McGreevy JP. 1991. Rock properties as controls on free-face debris fall activity. *Permafrost and Periglacial Processes* **2**: 311–319.

Evans SG, Hungr O. 1993. The assessment of rockfall hazard at the base of talus slopes. *Canadian Geotechnical Journal* **30**: 620–636.

Fisher O. 1866. On the disintegration of a chalk cliff. *Geological Magazine* **3**: 354–356.

Frich P, Brandt E. 1985. Holocene talus accumulation rates, and their influence on rock glacier growth: a case study from Igpik Disko, West Greenland. *Geografisk Tidsskrift* **85**: 32–44.
Gardner JS. 1969. Rockfall: a geomorphic process in high mountain terrain. *Albertan Geographer* **6**: 15–20.
Gardner JS. 1983. Rockfall frequency and distribution in the Highwood Pass area, Canadian Rocky Mountains. *Zeitschrift für Geomorphologie* **27**: 311–324.
Gerber E. 1980. Geomorphological problems in the Alps. *Rock Mechanics. Supplementum* **9**: 93–107.
Gerber E, Scheidegger AE. 1974. On the dynamics of scree slopes. *Rock Mechanics* **6**: 25–38.
Goodman RE. 1989. *Introduction to Rock Mechanics*. John Wiley and Sons: New York.
Goodman RE, Shi GH. 1985. *Block Theory and its Application to Rock Engineering*. Prentice-Hall: Englewood Cliffs, NJ.
Graf WL. 1971. The geomorphology of the glacial valley cross-section. *Arctic Alpine Research* **2**: 303–312.
Gray JT. 1972. Debris accumulation on talus slopes in the central Yukon Territory. In *Mountain Geomorphology*, Slaymaker HO, McPherson HJ (eds). Tantalus Press: Vancouver; 75–84.
Gruber S, Haeberli W. 2007. Permafrost in steep bedrock slopes and its temperature-related destabilization following climate change. *Journal of Geophysical Research* **112**. DOI: 10.1029/2006JF000547
Guido ZS, Ward DJ, Anderson RS. 2007. Pacing the post-Last Glacial maximum demise of the Animas Valley glacier and the San Juan Mountain ice cap, Colorado. *Geology* **35**: 739–742.
Guzzetti F, Reichenbach P, Wieczoreck GF. 2003. Rockfall hazard and risk assessment in the Yosemite Valley, California, USA. *Natural Hazards and Earth System Sciences* **3**: 491–503.
Guzzetti F, Crosta G, Detti R, Agliardi F. 2002. STONE: a computer program fro the three-dimensional simulation of rock-falls. *Computers and Geosciences* **28**: 1079–1093.
Hales TC, Roering JJ. 2005. Climate-controlled variations in scree production, Southern Alps, New Zealand. *Geology* **33**: 701–704.
Hales TC, Roering JJ. 2007. Climatic controls on frost cracking and implications for the evolution of bedrock landscapes. *Journal of Geophysical Research* **112**. DOI: 10.1029/2006JF000616
Harbor JM, Hallet B, Raymond CF. 1988. A numerical model of landform development by glacial erosion. *Nature* **333**: 347–349.
Harp EL, Tanaka K, Sarmiento J, Keefer DK. 1984. Landslides from the May 25–27, 1980, Mammoth Lakes, California, earthquake sequence, USGS Misc. Inv. Map I-1612. USGS: Reston, VA.
Hinchliffe S. 1999. Timing and significance of talus slope reworking, Trotternish, Skye, Northwest Scotland. *The Holocene* **9**: 483–494.
Hinchliffe S, Ballantyne CK. 1999. Talus accumulation and rockwall retreat, Trotternish, Isle of Skye, Scotland. *Scottish Geographical Journal* **115**: 53–70.
Hoffman T, Schrott L. 2002. Modelling sediment thickness and rockwall retreat in an Alpine valley using 2D-seismic refraction (Reintal, Bavarian Alps). *Zeitschrift für Geomorphologie, Suppl.-Bd*. **127**: 152–173.
Holzhausen GR. 1989. Origin of sheet structure, 1. Morphology and boundary conditions. *Engineering Geology* **27**: 225–278.
Huisman M, Hack HRGK, Nieuwenhuis JD. 2006. Predicting rock mass decay in engineering lifetimes: the influence of slope aspect and climate. *Environmental and Engineering Geoscience* **12**: 39–51.
Irigaray C, Fernandez T, Chacon J. 2003. Preliminary rock-slope-susceptibility assessment using GIS and the SMR classification. *Natural Hazards* **30**: 309–324.
Ishikawa M, Yoshimasa K, Kazuomi H. 2004. Analysis of crack movements observed in an alpine bedrock cliff. *Earth Surface Processes and Landforms* **29**: 883–891.
ISRM. 1978. Suggested Methods for determining rock hardness and abrasiveness of rocks. *International Journal of Rock Mechanics and Mining* **15**: 89–98.
Jaboyedoff M, Dudt JP, Labiouse V. 2005. An attempt to refine rockfall hazard zoning based on the kinetic energy, frequency and fragmentation degree. *Natural Hazards and Earth System Sciences* **5**: 621–632.
James LA, Harbor J, Fabel D, Dahms D, Elmore D. 2002. Late Pleistocene glaciations in the northwestern Sierra Nevada, California. *Quaternary Research* **57**: 409–419.
Krautblatter M, Dikau R. 2007. Towards a uniform concept for the comparison and extrapolation of rockwall retreat and rockfall supply. *Geografiska Annaler Series A* **89**: 21–40.
Koons PO. 1989. The topographic evolution of collisional mountain belts; a numerical look at the Southern Alps, New Zealand. *American Journal of Science* **289**: 1041–1069.
Luckman BH. 1976. Rockfalls and rockfall inventory data: some observations from Surprise Valley, Jasper National Park, Canada. *Earth Surface Processes and Landforms* **1**: 287–298.
Luckman BH. 1992. Debris flows and snow avalanche landforms in the Lairig Ghru Cairngorm mountains, Scotland. *Geografiska Annaler Series A* **74**: 109–121.
Mandl G. 2005. *Rock Joints*. Springer-Verlag: Berlin.
Marquinez J, Duarte RM, Farias P, Sanchez MJ. 2003. Predictive GIS-based model of rockfall activity in mountain cliffs. *Natural Hazards* **30**: 341–360.
Matsuoka N. 2001. Direct observation of frost wedging in alpine bedrock. *Earth Surface Processes and Landforms* **26**: 601–614.
Matsuoka N, Sakai H. 1999. Rockfall activity from an alpine cliff during thawing periods. *Geomorphology* **28**: 309–328.
Matthes FE. 1930. *Geologic History of the Yosemite Valley*, US Geological Survey Professional Paper 160. USGS: Reston, VA.
Matthes FE. 1938. Avalanche sculpture in the Sierra Nevada of California. *International Association of Scientific Hydrology Bulletin* **23**: 631–637.
McKean JA, Dietrich WE, Finkel RC, Southon JR, Caffee MW. 1993. Quantification of soil production and downslope creep rates from cosmogenic 10Be accumulations on a hillslope profile. *Geology* **21**: 343–346.
Miller DJ, Dunne T. 1996. Topographic perturbations of regional stresses and consequent bedrock fracturing. *Journal of Geophysical Research* **101**: 25523–25536.
Molnar P. 2004. Interactions among topographically induced elastic stress, static fatigue, and valley incision. *Journal of Geophysical Research* **109**. DOI: 10.1029/2003JF000097
Molnar P, Anderson RS, Anderson SP. 2007. Tectonics, fracturing of rock, and erosion. *Journal of Geophysical Research* **112**. DOI: 10.1029/2005JF000433
Moon V, Russell G, Stewart M. 2001. The value of rock mass classification systems for weak rock masses: a case example from Huntly, New Zealand. *Engineering Geology* **61**: 53–67.
Moore JR. 2007. *Rock Mass Strength Controls on the Erosion Rate of Alpine Cliffs in the Sierra Nevada, California, USA*. MS Thesis, University of California, Berkeley, CA.
Olyphant GA. 1983. Analysis of the factors controlling cliff burial by talus within Blanca Massif, Southern Colorado, USA. *Arctic Alpine Research* **15**: 65–75.
Phillips FM, Zreda MG, Benson LV, Plumber MA, Elmore D, Sharma P. 1996. Chronology for fluctuations in Late Pleistocene Sierra Nevada glaciers and lakes. *Science* **274**: 749–751.
Rapp A. 1960a. Recent development of mountain slopes in Kärkevagge and surroundings, northern Scandinavia. *Geografiska Annaler* **42**: 65–200.
Rapp A. 1960b. Talus slopes and mountain walls at Tempelfjorden, Spitsbergen. *Norsk Polarinstitutt Skrifter* **199**: 1–114.
Roering JJ, Kirchner JW, Dietrich WE. 1999. Evidence for non-linear, diffusive sediment transport on hillslopes and implications for landscape morphology. *Water Resource Research* **35**: 853–870.
Romana M. 1985. *New adjustment ratings for application of Bieniawski classification to slopes*. Proceedings of the International Symposium on the Role of Rock Mechanics: Zacatecas, Mexico; 49–53.
Romana M. 1995. *The geomechanical classification SMR for slope correction*. Proceedings of the Eighth International Congress on Rock Mechanics: Tokyo, Japan; 1085–1092.
Sass O. 2007. Bedrock detection and talus thickness assessment in the European Alps using geophysical methods. *Journal of Applied Geophysics* **62**: 254–269.
Sass O, Wollny K. 2001. Investigations regarding alpine talus slopes using ground-penetrating radar (GPR) in the Bavarian Alps, Germany. *Earth Surface Processes and Landforms* **26**: 1071–1086.
Saunders I, Young A. 1983. Rates of surface processes on slopes, slope

retreat and denudation. *Earth Surface Processes and Landforms* **8**: 473–501.

Savage WZ, Swolfs HS. 1986. Tectonic and gravitational stress in long symmetrical ridges and valleys. *Journal of Geophysical Research* **91**: 3677–3685.

Selby MJ. 1980. A rock mass strength classification for geomorphic purposes: with tests from Antarctica and New Zealand. *Zeitschrift für Geomorphologie* **24**: 31–51.

Selby MJ. 1982. Controls on the stability and inclinations of hillslopes formed on hard rock. *Earth Surface Processes and Landforms* **7**: 449–467.

Selby MJ. 1993. *Hillslope Materials and Processes*. Oxford University Press: Oxford.

Terzaghi K. 1962a. Stability of steep slopes on hard unweathered rock. *Geotechnique* **12**: 51–270.

Terzaghi K. 1962b. Dam foundation on sheeted granite. *Geotechnique* **12**: 199–208.

Tomkin JH, Braun J. 2002. The influence of alpine glaciation on the relief of tectonically active mountain belts. *American Journal of Science* **302**: 169–190.

Twidale CR. 1965. Weather pit (gnamma). *Australian Geographer* **9**: 318–319.

Walder J, Hallet B. 1985. A theoretical model of the fracture of rock during freezing. *Geological Society* of America *Bulletin* **96**: 336–346.

Weissel JK, Seidl MA. 1997. Influence of rock strength properties on escarpment retreat across passive continental margins. *Geology* **25**: 631–634.

Whalley WB. 1984. Rockfalls. In *Slope Instability*, Brunsden D, Prior DB (eds). John Wiley and Sons: Chichester; 217–256.

Wieczorek GF, Jäger S. 1996. Triggering mechanisms and depositional rates of postglacial slope-movement processes in the Yosemite Valley, California. *Geomorphology* **15**: 17–31.

Wieczorek GF, Morrissey MM, Iovine G, Godt J. 1999. *Rock-fall Potential in the Yosemite Valley, California*. US Geological Survey Open-file Report 99-578. USGS: Reston, VA.

DOI: 10.1002/esp